

The following is a preprint submitted to the journal Atmosphere-Ocean for peer review on October 10, 2024 (© 2025 under the [CC-BY-NC-ND 4.0 license](#)). A revised version was accepted on June 4, 2025. The definitive version from the publisher employs the title “A seasonal to decadal calibration of 1990–2100 eastern Canadian freshwater discharge simulations by observations, data models, and neural networks.” All versions seek to address:

- Calibration of the forcing (input), parameters (internal), and streamflow (output) of a hydrological model
- Relatively direct calibration of CMIP-forced simulations to observations
- Recognition of a familiar measurement modelling framework at each step

A seasonal to decadal calibration of 1990–2100 eastern Canadian freshwater discharge simulations by observations, data models, and neural networks

Richard E. Danielson^{1,2}, Minghong Zhang², Joël Chassé¹, and Will Perrie²

¹Fisheries and Oceans Canada, Gulf Fisheries Centre, Moncton, New Brunswick;

²Fisheries and Oceans Canada, Bedford Institute of Oceanography, Dartmouth, Nova Scotia, Canada

Keywords: watershed hydrology; process model; calibration; data model; climate trends

Abstract

A configuration of the NCAR WRF-Hydro model was sought using well established data models to guide the initial hydrologic model setup, as well as a seasonal streamflow post-processing by neural networks. Discharge was simulated using an eastern Canadian river network at two-km resolution. The river network was taken from a digital elevation model that was made to conform to observed catchment boundaries. Perturbations of a subset of model parameters were examined with reference to streamflow from 25 gauged catchments during the 2019 warm season. A data model defines the similarity of modelled streamflow to observations, and improvements were found in about half the individual catchments. With reference to 183 gauged catchments (1990-2022), further improvements were obtained at monthly and annual scales by neural network post-processing that targets all catchments at once as well as individual catchments.

This seasonal calibration was applied to uncoupled WRF-Hydro simulations for the 1990-2100 warming period. Historic and future forcing were provided, respectively, by a European Centre for Medium-Range Weather Forecasting reanalysis (ERA5), and by a WRF atmospheric model downscaling of a set of Coupled Model Intercomparison Project (CMIP) models, where the latter were also seasonally calibrated. Eastern Canadian freshwater discharge peaks at about $10^5 \text{ m}^3 \text{ s}^{-1}$, and as previous studies have shown, there is a trend toward increasing low flows during the cold season and an earlier peak discharge in spring. By design, neural networks yield more precise estimates by compensating for different hydrologic process representations.

1 Introduction

Anticipation of future changes in the water cycle depends in part on hydrologic model simulations that are capable of reproducing historical river discharge estimates. [Bush and Lemmen \(2019\)](#) summarize climate projections for Canada, as well as ongoing changes in the water cycle as global temperature rises. Precipitation may have already increased across northern Canada, and while less of this is frozen, the total amount is expected to increase further through 2100, particularly in winter ([Zhang et al. 2019b](#)). Permafrost temperature is also increasing as the duration of land and marine snow and ice cover decreases ([Derksen et al. 2019](#)). Cold season river discharge is expected to continue increasing, with an earlier peak discharge in spring ([Bonsal et al. 2019](#)). Concurrently, surface density stratification may be changing in Canadian waters ([Greenan et al. 2019](#)).

The hydrologic component of the water cycle begins with precipitation reaching the ground and ends with catchment loss, either by evaporation or discharge to the ocean ([Beven 2019](#)). Hydrologic simulations are needed to assess the downstream impact of temperature and precipitation changes on streamflow and ocean stratification. Increasing and earlier peak river discharge trends are found by [Stadnyk et al. \(2021\)](#) in Arctic simulations that cover 1981-2070 using the Hydrological Predictions for the Environment (HYPE) model of the Swedish Meteorological and Hydrological Institute (SMHI). As hydrologic models are sensitive to bias in the forcing used for calibration ([Berg et al. 2018](#)), atmospheric forcing for 1981-2010 is taken from the Hydrological Global Forcing Data (HydroGFD), which in turn, is a calibration reference for 2011-2070 forcing by Earth System models ([Taylor et al. 2012](#); [IPCC 2013](#)) of the Coupled Model Intercomparison Project (CMIP). [Stadnyk et al.](#) also perform ocean simulations for 2002-2009 using the Nucleus for European Modelling of the Ocean (NEMO) model. Their comparison of high-latitude forcing from HYPE and from observed estimates of monthly-mean streamflow ([Dai et al. 2009](#)) points to a hydrologic contribution to ocean stratification changes.

Components of Earth System models that provide operational forecasts are known to perform well against observations ([Schmidt et al. 2017](#)). Like HYPE, the National Center for Atmospheric Research (NCAR) Weather Research and Forecasting (WRF) hydrologic model (WRF-Hydro; [Gochis et al. 2021](#)) is employed in operations. The natural representa-

tions that WRF-Hydro employs include column land surface (NOAH-MP), subsurface flow, and overland flow components that drive the main discharge to the ocean via a river and lake network ([Gochis et al. 2021](#)). Streamflow routing follows a river network that the WRF-Hydro preprocessor interpolates from a digital elevation model (DEM). The subkilometer resolution of most DEMs may be appropriate in operations, but [Eilander et al. \(2021\)](#) provides an upscaled DEM that preserves river structure at lower resolution. Moreover, [Lehner et al. \(2008\)](#) provide watershed boundaries to preserve an interpolated catchment area upstream of hydrologic stations ([de Rham et al. 2020](#); [Pellerin and Nzokou Tanekou 2020](#)). With a river network that reproduces the natural network as closely as possible, both in terms of station location and upstream area, it is easier to associate WRF-Hydro simulations with observations.

A calibration to observations can be seen as *anchoring* a hydrologic model when both its internal processes, and the variables it shares with adjacent Earth system models, more closely mimic nature ([Schmidt et al. 2017](#); [Stadnyk et al. 2020](#)). Regarding upstream atmospheric forcing, its calibration is expected to depend on the individual CMIP model ([Berg et al. 2018](#)), but also should allow for the synoptic evolution of a freely evolving climate model, which is different than in observations ([Maraun 2016](#)). Not only does multivariate bias correction address such upstream issues, but notably, it also preserves decadal trends ([Cannon 2018](#)), although the temporal sequence of CMIP forcing is adjusted slightly to match the probability distributions of observations. We return to this issue in Section 3.d, where we seek to associate simulated and observed streamflow without matching synoptic sequences.

Regarding internal parameters of a hydrologic model (and Earth system models generally), the identification of unique values for an increasing number of parameters is another known challenge ([Schmidt et al. 2017](#); [Beven 2021](#)). If computer resources are well allocated ([Wang et al. 2019](#)), then automatic calibration offers a partial solution ([Doherty 2015](#)). A comprehensive calibration of parameters in HYPE is given by [Stadnyk et al. \(2020\)](#), who develop multiyear simulations of discharge to Hudson Bay, with representations of lake storage and frozen soil. Examples of automatic calibration of WRF-Hydro include [Wang et al. \(2019\)](#) and [Rafieei Nasab et al. \(2020\)](#), who rely on objective functions similar to those of [Stadnyk et al.](#) to identify model parameters.

Step	Process Model	Representation	Reference	Data Model	Calibration
1	Topographic	Watershed boundaries	HydroSHEDS	Truth	Section 3a
1	Atmospheric	Downscaled CMIP forcing	ERA5	Truth	Section 3b
3	Hydrologic	WRF-Hydro parameters	HyDAT	Target	PEST
4	Hydrologic	WRF-Hydro streamflow	HyDAT	Target	Neural network

Table 1: Summary of calibration steps applied in this study and the type of representation involved, along with the choice of reference, data model, and method of calibration (see text for definitions).

Regarding downstream ocean forcing, calibration of the output of a hydrologic model can help to address river regulation and streamflow buffering by many small lakes in eastern Canada (Déry et al. 2018; Staden et al. 2020). If observations are available, then advances in neural network training (Rumelhart et al. 1986; Innes et al. 2018) enable automatic calibration of generic model structures, which can be used to relate simulated and observed streamflow at gauged stations furthest downstream, and at eastern Canadian ocean outlets (Dai and Trenberth 2002). Stiles et al. (2014) demonstrates that a composition of neural networks can be used to target different aspects of a relationship. However, because they offer a parameterized nonlinear relationship between WRF-Hydro and HyDAT streamflow, it is not obvious that decadal trends are preserved (Maraun 2016; Cannon 2018).

Hydrologic models are expected to require calibration following any change in configuration, including going from an operational resolution of one km or less to climate simulations at coarser resolution. Within an Earth system modelling framework, each calibration step upstream, internal, and downstream of WRF-Hydro is important. The steps taken in this study are shown in Table 1, beginning with enforcing watershed boundaries and with a seasonal calibration of atmospheric forcing. This is followed by hydrologic calibration using an automatic parameter estimation tool called PEST (Doherty 2015; Wang et al. 2019). Calibration of WRF-Hydro streamflow is then explored using neural networks (Stiles et al. 2014; Innes et al. 2018). As ocean forcing is emphasized below, we focus increasingly on the hydrologic steps, using observed discharge from eastern Canadian rivers as our reference. Methods and results are provided for each calibration step in Sections 3 and 4, respectively. A discussion is given in Section 5 and

conclusions are given in Section 6. The next section describes the observed and simulated data.

2 Data

Hydrologic processes are represented by WRF-Hydro on a grid projection at two resolutions (Fig. 1). We obtain unadjusted atmospheric and topographic data from a western North Atlantic downscaling of multi-year CMIP simulations (Zhang et al. 2019a) and a global upscaled DEM (Eilander et al. 2021) at horizontal grid resolutions of 30 km and 1 km, respectively. Slightly lower resolutions of 50 km and 2 km are selected for the WRF-Hydro land surface model (54 by 62) and river routing (1350 by 1550) grids covering eastern Canada.

2.1 Topographic data

Surface elevation from satellites requires adjustment before a river network can be derived that matches observed paths and flow directions (Lehner et al. 2008; Yamazaki et al. 2019). The WRF-Hydro preprocessor performs bilinear interpolation of a DEM to the routing grid, but the resulting river network and watershed boundaries are sensitive to the input DEM resolution. Using the hydrologically adjusted DEM of Yamazaki et al. (2019), Eilander et al. (2021) develop an iterative approach to representing river structure, length, and slope at lower resolution. Reliance on interpolation is reduced as this DEM is at slightly higher resolution than the WRF-Hydro routing grid. To ensure that catchment areas upstream of hydrologic stations are also preserved, watershed boundaries in the 15-arcsec HydroSHEDS DEM (Lehner et al. 2008) are employed as a reference.

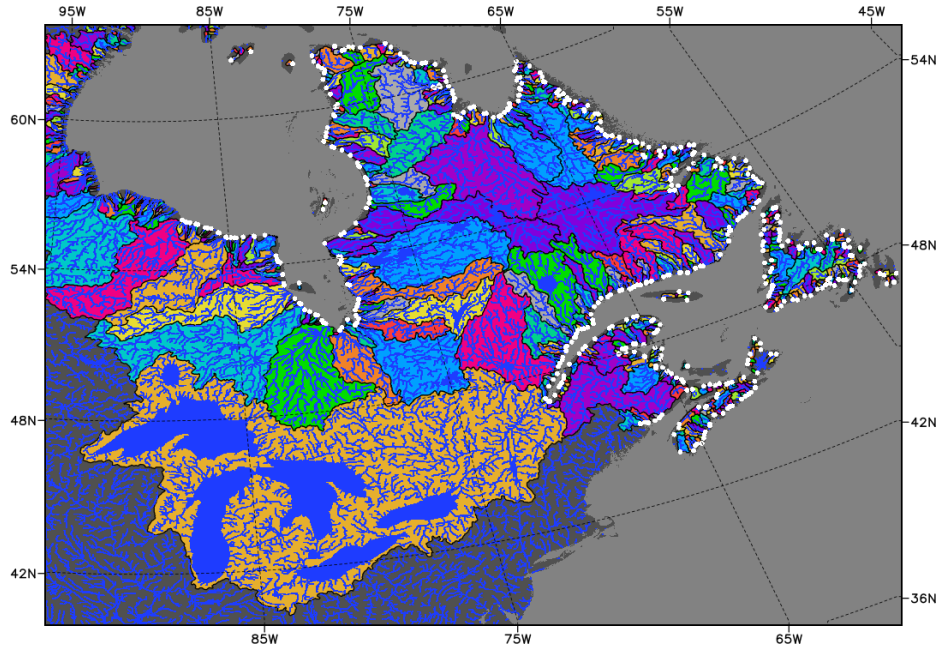


Figure 1: Native WRF-Hydro projection (Lambert conformal conic) of the eastern Canadian 50-km (54×62) land surface model and 2-km (1350×1550) river routing grids, with a river and lake network (dark blue) that discharges from watersheds (colours) to the ocean at 477 outlets between the Severn (Ontario) and St. Croix (New Brunswick/Maine) rivers (white dots).

2.2 Atmospheric data

A useful reference for historical CMIP simulations is a reanalysis of observed atmospheric forcing (Stadnyk et al. 2021). We employ the fifth European Centre for Medium-Range Weather Forecasting Reanalysis (ERA5; Hersbach et al. 2020), which is based on a spectral model (137 vertical levels and an effective horizontal resolution of 31 km) with data assimilation over successive 12-h periods, and a reduction in systematic differences between the model and observations (Dee 2005). This global atmospheric reference is available hourly on a 0.25° grid, and we bilinearly interpolate three-hourly surface forcing for 1990-2022 to the 50-km WRF-Hydro grid (Fig. 1).

Our representations of historical and future forcing are a combination of low resolution CMIP simulations (Flato et al. 2019) and enhanced (30-km) resolution by a Weather Research and Forecasting (WRF) model downscaling (Zhang et al. 2019a). A standard hydroclimatic assessment may employ 15 representations or more, but we employ four, where WRF is driven at lateral and lower boundaries by a selected Earth System simulation that, in turn, is driven by a shared socioeconomic pathway (SSP2-4.5 or SSP5-8.5) scenario (O'Neill et al. 2017). We employ three simulations from the CMIP5 experiment (Taylor et al. 2012) and one from CMIP6 (Eyring et al. 2016). Respectively, these are an NCAR Community

Climate System Model (CCSM-4 SSP5-8.5) simulation (Meehl et al. 2012), two Met Office Hadley Centre Global Environmental Model (HadGEM2 SSP2-4.5 and SSP5-8.5) simulations (Collins et al. 2011), and a Max Planck Institute for Meteorology Earth System Model (MPI-ESM1.2-LR SSP5-8.5) simulation (Mauritsen et al. 2019). Each six-hourly representation for 1990-2100 is also bilinearly interpolated to the 50-km grid.

2.3 Hydrologic data

Instrumental daily streamflow serves as a useful reference for calibrating WRF-Hydro parameters and output, although from day to day, streamflow itself is not measured at most eastern Canadian hydrologic stations. Instead, river stage (i.e., water level) is monitored and daily streamflow is obtained from stage-discharge relationships that depend in part on open-water or ice-affected conditions (de Rham et al. 2020). These streamflow observations are taken from HyDAT, the National Water Data Archive of the Water Survey of Canada (2023). For WRF-Hydro parameter calibration (Section 3.c), we focus on Reference Hydrometric Basin Network (RHBN) stations (Pellerin and Nzokou Tanekou 2020), which are a HyDAT subset with long records (>20 years) and little or no impact from upstream dams and reservoirs.

3 Methods

We begin with the conventional assumption that calibrations based on historical data can be applied well into the future (Maraun 2016). Two initial calibration steps are done in parallel (Table 1) that seek to reproduce a natural river network and perform a seasonal atmospheric calibration. We then perform hydrologic calibration, first using a parameter estimation tool called PEST (Doherty 2015; Wang et al. 2019), and next by discharge post-processing using neural networks (Stiles et al. 2014; Innes et al. 2018). These two steps are similar in that discharge from large catchments involves nonlinear contributions by many concurrent processes, and both PEST and neural networks accommodate process nonlinearity. Moreover, both calibration steps are performed with reference to daily streamflow (Pellerin and Nzokou Tanekou 2020) and employ the same data model. This data model is manifest in the PEST objective function and the neural network loss function, where minima in the difference between predicted and observed streamflow are sought. Data models are defined in the Appendix, with the calibrated reference and uncalibrated representation (e.g., HyDAT observed and WRF-Hydro predicted streamflow) denoted by C and U , respectively.

3.1 Topographic calibration

To compare streamflow at HyDAT stations and on the WRF-Hydro routing grid, we ensure that upstream catchment areas are comparable. Thus, watershed boundaries are located in the 15-arcsec HydroSHEDS DEM (Lehner et al. 2008) and the same boundaries are imposed in WRF-Hydro by raising DEM values by $O[100 \text{ m}]$. This is done before interpolation and upstream of selected inland stations in Section 4.c, and after interpolation and upstream of all outlets to the ocean in Section 4.d. Either inland or coastal adjustment is employed (not both) to make the WRF-Hydro river network and watersheds similar to HydroSHEDS. For this calibration, it suffices to treat the HydroSHEDS boundaries (C) as if they were fixed and natural. The truth model is employed, but we only confirm visually that the distance between C and U is smaller when the HydroSHEDS boundaries are imposed (Section 4.a).

3.2 Atmospheric calibration

A seasonal calibration using ERA5 as a reference is applied to atmospheric forcing after interpolation to the WRF-Hydro 50-km land surface grid (Section 2.b). In addition to CMIP model downscaling using the same atmospheric model (Zhang et al. 2019a), this cal-

ibration helps to address systematic differences among CMIP models (Flato et al. 2019). Averages are taken over land in Fig. 1 and for each day of the year between 1990 and 2004, and the resulting annual cycle is approximated by a sinusoid (Jacquelin 2014). These smooth annual cycles define a daily linear adjustment to ERA5 that is applied to all years (1990-2100). Calibration is multiplicative for wind speed and precipitation, additive for other variables, and some forcing variables are omitted if a more sophisticated calibration is required (i.e., for shortwave and longwave radiation), or differences with ERA5 are small. Again for this calibration, it suffices to treat the smooth annual cycle of ERA5 (C) as fixed and natural. The truth model is also employed and we confirm visually that $C - U$ is smaller after calibration (Section 4.b).

3.3 Hydrologic model calibration

The WRF-Hydro model is a parallelized, distributed process model (Gochis et al. 2021), whose core components (and our specific settings) are a column land surface model (four-layer Noah-MP), overland flow (steepest descent), shallow subsurface flow (saturated flow), groundwater baseflow (exponential bucket), channel routing (diffusive wave), and reservoir routing (level-pool). Simulations employ land surface and river routing timesteps of 1 h and 30 sec, respectively. The automatic parameter estimation tool PEST (Doherty 2015) is employed to tune WRF-HYDRO parameters to yield a similarity to observations. For the conterminous U.S., Rafeei Nasab et al. (2020) provide the range and sensitivity of a number of WRF-Hydro parameters, of which nine are selected for calibration (Table 2).

This calibration ignores CMIP data, and instead estimates parameters using the coordinated synoptic evolution of ERA5 forcing and HyDAT streamflow. A three-year WRF-Hydro spinup is performed using annual-mean ERA5 forcing, and a baseline simulation is performed from October 1, 2018 to October 31, 2019 using default parameters. Following Wang et al. (2019), over 100 WRF-Hydro simulations are then launched during parameter estimation. Each begins with a restart from the baseline simulation on March 31, 2019. The PEST objective function (Φ_P) is evaluated using model and observed streamflow differences between May and October. Apart from WRF-Hydro itself, the only process (i.e., “expert”) knowledge given to PEST is the acceptable range in each free parameter (Rafeei Nasab et al. 2020). In other words, we employ PEST’s “estimation mode” and omit prior information and additional process knowledge (i.e., Tikhonov regularization). The objective function minimization employs singular value decomposition (SVD) for numerical stability (Doherty 2015).

Parameter	Description	Range	PEST Value
BEXP	Coefficient of pore size distribution	$\times [0.4, 1.9]$	0.47
DKSAT	Saturated hydraulic conductivity (m s^{-1})	$\times [0.2, 10.0]$	0.21
MFSNO	Snow depletion melt	$[0.5, 3.0]$	0.50
MP	Slope of Ball-Berry conductance	$\times [0.6, 1.4]$	1.40
OVROUGHRTFAC	Manning’s roughness for overland flow	$[0.5, 1.5]$	1.50
REFKDT	Infiltration/surface runoff partitioning	$[0.1, 4.0]$	0.68
RETDEPRTFAC	Maximum retention depth	$[0.1, 10.0]$	0.23
SLOPE	Bottom drainage boundary	$[0.0, 1.0]$	0.27
SMCMAX	Saturated soil moisture content	$\times [0.8, 1.2]$	1.02

Table 2: Nine WRF-Hydro calibration parameters, as in [Rafieei Nasab et al. \(2020\)](#), with corresponding descriptions, ranges, and PEST values (bold values are close to a range limit; see Section 4.c). All parameter values are spatially constant, but ranges that begin with \times multiply a spatially varying default field.

The guided search for WRF-HYDRO parameters (Table 2) leads to a greater similarity to streamflow observations, which is a well established definition of improvement. Although PEST and neural networks are different methods of calibration, when deriving their objective or loss function, they share the same target data model and make the same *equivalence assumption* between C and U (see Appendix). For PEST, the basic function that guides the parameter search is

$$\Phi_P = [C-U]^T Q^{-1} [C-U], \quad (1)$$

where C and $U = Xp$ are streamflow (X is a linear representation of the WRF-Hydro model and p contains the parameter values), and Q corresponds to a HyDAT and WRF-Hydro error covariance matrix. We consider minimization of Φ_P to be complete after five iterations, each of which usually employs more than 20 WRF-Hydro simulations ([Doherty 2015](#)).

3.4 Hydrologic data calibration

The specific configuration of WRF-Hydro that is employed in this study may limit the physical processes that are simulated, and we would not expect a subsequent calibration to compensate for missing processes. Notable challenges in eastern Canada include the prevalence of small lakes, frozen soil, and river regulation ([Déry et al. 2018](#); [Stadnyk et al. 2020](#)). Insofar as processes are lacking in our simulations, however, we also expect these to have a systematic nonlinear impact on the processes that are both a) captured by HyDAT observations, and b) simulated by WRF-Hydro but without being impacted. It is by way of a parameterized nonlinear relationship between WRF-Hydro and HyDAT streamflow that we propose a subsequent calibration of WRF-Hydro output.

Neural networks are adaptive and convenient for identifying a nonlinear relationship when some of the physical processes involved are not apparent. In ad-

dition to process differences, CMIP model forcing is freely evolving, so WRF-Hydro and HyDAT streamflow are asynchronous on synoptic scales. [Stiles et al. \(2014\)](#) demonstrates that a composition of neural networks can capture different aspects of a relationship, so two neural networks are employed. The first (NN232 hereafter) seeks to “buffer” streamflow by reducing strong peaks in both seasonal and daily flows. Thus, we design its input and output layers to have two nodes for daily streamflow and a 12-day centered average. Between these layers is a three-node hidden layer with batch normalization, a dense connection between all layers, and an ELU activation function at each connection ([Clevert et al. 2015](#)).

The second neural network (NN343 hereafter) provides a nonlinear parameterization of a) missing processes like river regulation and b) the freely evolving synoptic-scale forcing of each CMIP model. We design its input and output layers to have three nodes for daily, monthly, and annual-mean streamflow, with dense connections to a four-node hidden layer with batch normalization. Of course, (b) does not pertain to ERA5 forcing, since WRF-Hydro and HyDAT streamflow would be synchronized. However, a synoptic pairing of daily data is not possible when training separately for each CMIP model, and in that case, we allow for an asynchronous synoptic evolution. Following [Freilich and Challenor \(1994\)](#), ranked daily flows in WRF-Hydro and HyDAT are matched (but the order of the monthly and annual-mean input and output data are unchanged). The result is a seasonally calibrated streamflow whose temporal sequence is unaltered (cf. [Maraun 2016](#); [Cannon 2018](#)).

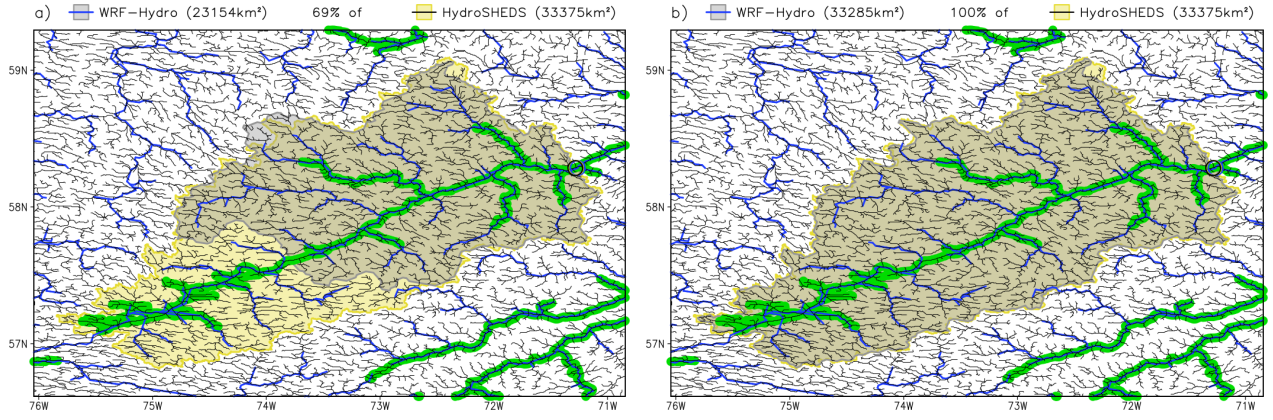


Figure 2: Catchment area upstream of hydrologic station 03JB004 (Rivière Aux Feuilles, upstream of Dufreboy Brook) following an interpolation of the 30-arcsec DEM of [Eilander et al. \(2021\)](#) to the 2-km WRF-Hydro grid a) before and b) after raising the height of the input DEM by 100 m at the 15-arcsec HydroSHEDS catchment boundary ([Lehner et al. 2008](#)). Shown are the station (circle), WRF-Hydro rivers (blue) and catchments (grey), HydroSHEDS rivers (black) and catchments (yellow), and rivers wider than about 30 m from Landsat images (green; [Altenau et al. 2021](#)).

The number of parameters sought for NN232 (23) and NN343 (39) is more than for WRF-Hydro (9), and as in (1), guided searches lead to a greater similarity to observations. A similar loss function (Φ_N) is also used for training:

$$\Phi_N = [C - U]^T [C - U]. \quad (2)$$

Parameter solutions are obtained using Flux.jl ([Innes et al. 2018](#)) and we consider minimization complete after 1000 iterations. Although neural networks provide two or three outputs (e.g., daily, monthly, and annual-mean), only daily streamflow is retained. Finally, because neural networks are trained at inland gauged stations, we also apply them to WRF-Hydro discharge at the coast, where they provide a nonlinear calibration (cf. [Dai and Trenberth 2002](#)).

3.5 Hydrologic performance

One composite measure of performance is employed, following [Moriiasi et al. \(2015\)](#), who define a satisfactory comparison at a gauged station as having a difference (DIFF) between WRF-Hydro and HyDAT of 15% or less and Nash-Sutcliffe efficiency (NSE) of 0.5 or greater. The individual expressions of accuracy and skill are $\text{DIFF} = \Sigma|U - C|/\Sigma|C|$, $\text{NSE} = 1 - \Sigma(U - C)^2/\Sigma(C - \bar{C})^2$, root-mean-square difference (RMSD) $= (\Sigma(U - C)^2/n)^{0.5}$, bias (BIAS) $= \Sigma(U - C)/n$, and Pearson correlation (COR) $= \Sigma(U - \bar{U})(C - \bar{C})/(\Sigma(C - \bar{C})^2 \Sigma(U - \bar{U})^2)^{0.5}$. As in (1) and (2), all but Pearson correlation seem to take C and U to be equivalent.

4 Results

4.1 Topographic calibration

Interpolation of the 30-arcsec hydrologically conditioned DEM of [Eilander et al. \(2021\)](#) to the 2-km WRF-Hydro routing grid did not always ensure that catchment area upstream of a hydrologic station or an ocean outlet was fully captured. An example of topographic processing for hydrologic station 03JB004 (Rivière Aux Feuilles, upstream of Dufreboy Brook) is shown in Fig. 2a, but catchments at other stations also differed (not shown). The 30-arcsec and 2-km resolutions are close, so much of the effort to preserve river structure from higher resolution ([Eilander et al. 2021](#)) was retained on the WRF-Hydro grid. This is apparent by the overlap among three different river networks. Imposing HydroSHEDS catchment boundaries (Fig. 2b) allowed an area occupied by Qasigialik (Lake Minto) to drain eastward to Ungava Bay instead of westward to Hudson Bay. HydroSHEDS errors notwithstanding, we ensured that runoff would be routed to the appropriate ocean outlet (Fig. 1) to support WRF-Hydro and HyDAT streamflow associations.

WRF-Hydro forcing	CCSM-4 SSP5-8.5	HadGEM2 SSP2-4.5/5-8.5	MPI-ESM1.2-LR SSP5-8.5
Precipitation (mm hr^{-1})	$\times [1.0, 1.2]$	$\times [0.9, 1.2]$	
Temperature ($^{\circ}\text{C}$)	$- [0.3, 2.7]$	$+ [2.1, 2.9]$	
Specific Humidity (g kg^{-1})	$- [0.2, 0.6]$		
Wind Speed (m s^{-1})	$\times [0.9, 1.0]$	$\times [0.8, 0.9]$	$\times [1.0, 1.1]$
Surface Pressure (hPa)	$- [0.8, 3.1]$		

Table 3: Range of daily linear adjustments applied to downscaled CMIP simulations, where $+/-$ and \times refer to additive and multiplicative adjustments, respectively. Shortwave and longwave radiation (not adjusted) are the remaining WRF-Hydro forcing variables.

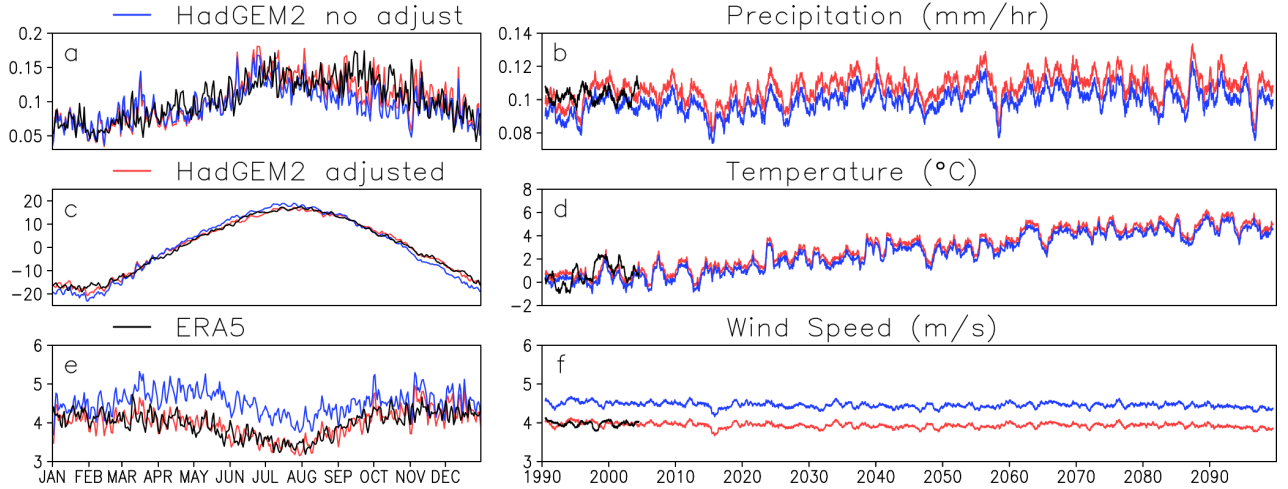


Figure 3: Linear adjustment of HadGEM2 to ERA5 (left panels) based on averages over land in Fig. 1 and for each day of the year between 1990 and 2004, and (right panels) applied to SSP2-4.5 annual averages for 1990-2100. Shown are a,b) precipitation (mm hr^{-1}), c,d) temperature ($^{\circ}\text{C}$), and e,f) wind speed (m s^{-1}). Note that the same historical adjustments are applied to HadGEM2 SSP5-8.5.

4.2 Atmospheric calibration

Table 3 lists the range in additive and multiplicative adjustments that were applied to the downscaled atmospheric forcing of WRF-Hydro. Five, three, and one WRF-Hydro variables were adjusted for CCSM-4, HadGEM2, and MPI-ESM1.2-LR, respectively, with no adjustment of shortwave and longwave radiation. Adjustments for HadGEM2 are shown in Fig. 3, which reveals a deficit in precipitation during September and October, and a warm-season surplus in wind speed (blue lines in Fig. 3a,e), whose adjustments (red lines) are reflected in annual averages (Fig. 3b,f). Relative to ERA5, CCSM-4 precipitation was also deficient in fall (not shown). Although we ignored ERA5 errors (e.g., any wind speed reference might be biased low in storms), as expected, linear adjustments preserved the timing of synoptic forcing (i.e., at 1-10 days) and simulated trends in eastern Canada (Maraun 2016; Bush and Lemmen 2019).

4.3 Hydrologic model calibration

We sought a representation of *natural flow* through our river network in an automatic calibration of WRF-Hydro parameters. As the Reference Hydrometric Basin Network (RHBN) stations are HyDAT stations with little or no impact from upstream dams and reservoirs (Pellerin and Nzokou Tanekou 2020), we selected 25 RHBN stations with the largest upstream catchments (Fig. 4), where 3699 streamflow observations were taken between the end of May and October 2019. The WRF-Hydro watershed boundaries were adjusted to match HydroSHEDS (Section 3.a), lakes were omitted, and ERA5 atmospheric forcing was employed at 6-h intervals.

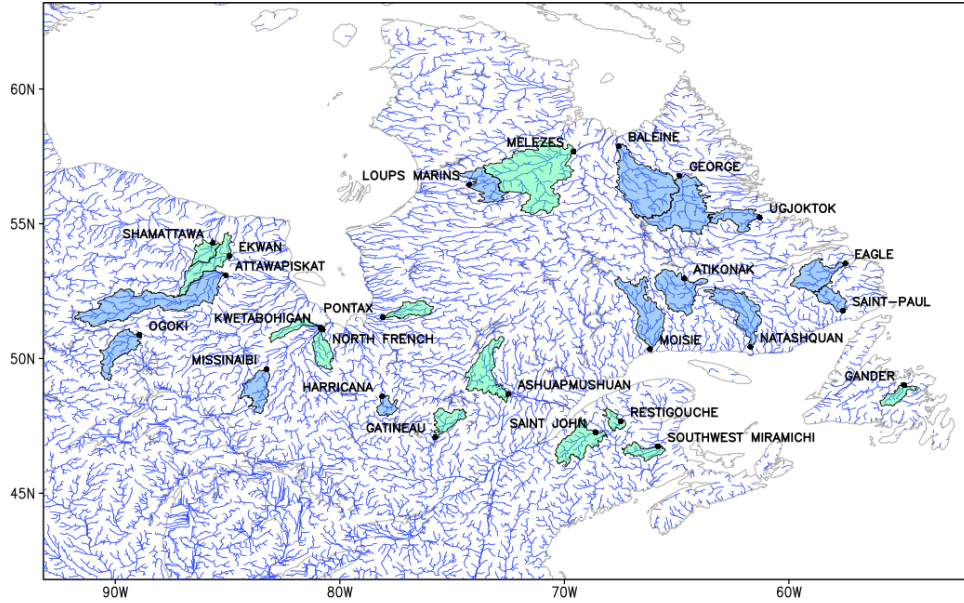


Figure 4: Catchments (shaded) upstream of 25 Reference Hydrometric Basin Network stations (black dots), where 3699 daily observations are available between May 31 and October 30, 2019. Catchment shading denotes an increase (blue) or decrease (green) in WRF-Hydro similarity to observations (i.e., Nash-Sutcliffe efficiency) when going from default to PEST values for nine WRF-Hydro parameters (Table 2). Each station provides 153 observations, except for 03BF001/Pontax (63) and 03KC004/Mélèzes (117). Also shown is the 2-km WRF-Hydro river network with lakes omitted (blue lines).

Nine WRF-Hydro parameters (Table 2) were calibrated using PEST, and although all are allowed to vary spatially (Gochis et al. 2021), we employed (or multiplied by) constant values across the eastern Canadian domain. This calibration was challenging because other WRF-Hydro parameters were fixed, including Manning’s roughness coefficients for rivers (cf. Wang et al. 2019). We initially assumed, *but did not confirm*, that a natural-flow representation could be identified for the entire eastern Canadian domain, as many parameters given by PEST were close to their limit in range of application (bold values in Table 2). Moreover, in going from default to PEST parameter values, we obtained greater similarity to observations (i.e., Nash-Sutcliffe efficiency) at only 13 of the 25 RHBN stations (Fig. 4).

A comparison of streamflow at individual stations revealed that the HyDAT/RHBN observations varied more smoothly than WRF-Hydro predictions, which captured strong peaks in both seasonal and daily flows using default and PEST parameters. Figure 5 is an example of streamflow at the Attawapiskat River station (Figure 4), where default parameters overestimate the spring freshet in May and PEST parameters overestimate two peaks in July. A simulation of strong daily flows seems consistent with our PEST values of low soil infiltration (REFKDT) and reten-

tion (RETDEPRTFAC), and high surface roughness (OVROUGHRTFAC; Table 2), but also, RHBN stations capture streamflow buffering by small lakes upstream (Stadnyk et al. 2020), whereas no lakes were included in our PEST simulations.

4.4 Hydrologic data calibration

Before seeking a representation of *natural and regulated flow* for individual catchments using neural networks, we first sought to extend the calibration of natural flow for all catchments uniformly. Starting with the PEST parameters obtained above, we considered a calibration to address strong peaks in the seasonal and daily flows of the 25 RHBN stations (Fig. 4). The NN232 neural network (using daily and 12-day average streamflow) was trained to associate WRF-Hydro with the 3699 RHBN observations. Table 4 reveals that even using NN232 streamflow, only two of 25 stations were considered satisfactory (Moriassi et al. 2015), but as expected, NN232 also yielded adjustments that smoothed, and in part buffered, streamflow where peaks in the daily and 12-day averages were different. At the Attawapiskat River station (Fig. 5), PEST discharge (purple) was more similar to HyDAT (black) than default WRF-Hydro parameters (orange), and the largest flows were further reduced by NN232 (grey), which was more similar by design.

Parameter Setting	Satisfactory Stations	DIFF (%)	NSE	COR
Default	2	50	-0.86	0.69
PEST	2 (13)	57	-0.60	0.70
NN232	2 (19)	32	0.24	0.74

Table 4: Summary of the similarity between HyDAT and WRF-Hydro streamflow using default parameters, PEST parameters, and PEST parameters with neural network (NN232) post-processing (i.e., training and testing employ the same reference). Averages over 25 stations are given for the absolute value of model-observation difference (DIFF, as a percent of observed streamflow), Nash-Sutcliffe efficiency (NSE), and Pearson correlation (COR; see Section 3.e for definitions). Included are the number of satisfactory stations (NSE>0.5 and DIFF<15%) and number of stations with improved NSE relative to default (in brackets).

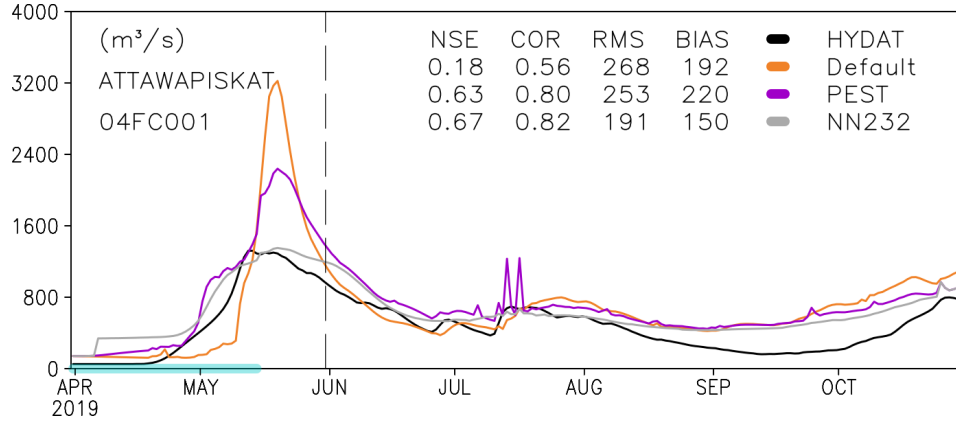


Figure 5: Daily discharge ($\text{m}^3 \text{s}^{-1}$) during 2019 at Attawapiskat River below Muketei River (04FC001), as given by HyDAT (black) and WRF-Hydro, where the latter employs default (orange) and PEST (purple) parameters, and after PEST discharge is post-processed using a neural network (NN232; grey). Included are values of Nash-Sutcliffe efficiency (NSE), Pearson correlation (COR), root-mean-square difference (RMS), and bias (BIAS) of WRF-Hydro with reference to HyDAT for discharge between May 31 (dashed line) and October 30. Blue shading (abscissa) denotes a backwater ice impact on HyDAT water level.

As multiple neural networks can be chained together (Stiles et al. 2014), we used NN232 as a baseline for the NN343 calibration of individual catchments. Many large rivers in eastern Canada are regulated, and regardless of atmospheric forcing, the need for separate seasonal calibrations is apparent. Regulated flows of the St. Lawrence and Churchill Rivers are shown in Fig. 6. Spring peaks in WRF-Hydro (grey) often exceed those in HyDAT (black), and as expected, regulated HyDAT flow is otherwise larger for the remainder of the year. Similarity among CMIP simulations and their systematic differences with HyDAT are more apparent in the annual averages (Fig. 6c,f). Neural network calibration is shown here to demonstrate that the largest flows (NN232, orange lines) and seasonal differences (NN343, purple lines) are reduced, although adjustments at both stations are incomplete. That is, HyDAT station 02OA016 is a partial measure of St. Lawrence streamflow (Morin and Champoux 2006), and for Churchill, NN343 is slow to capture

the flow increase in early May and a return to low flow in July-October.

For all remaining WRF-Hydro simulations, we adjusted watershed boundaries upstream of the 477 ocean outlets (Section 3.a) and included 20 lakes larger than 1000 km^2 (Messenger et al. 2016). Although lake shapefiles were also adjusted to match the 2-km river routing grid, inside these lakes we replaced time-invariant surface characteristics (in geogrid.nc) with adjacent land values. This was done to ensure the stability of long-running simulations, but contributed to systematic differences inherited by the NN343 calibration, with low flow in the St. Lawrence (Fig. 6c) being an obvious example.

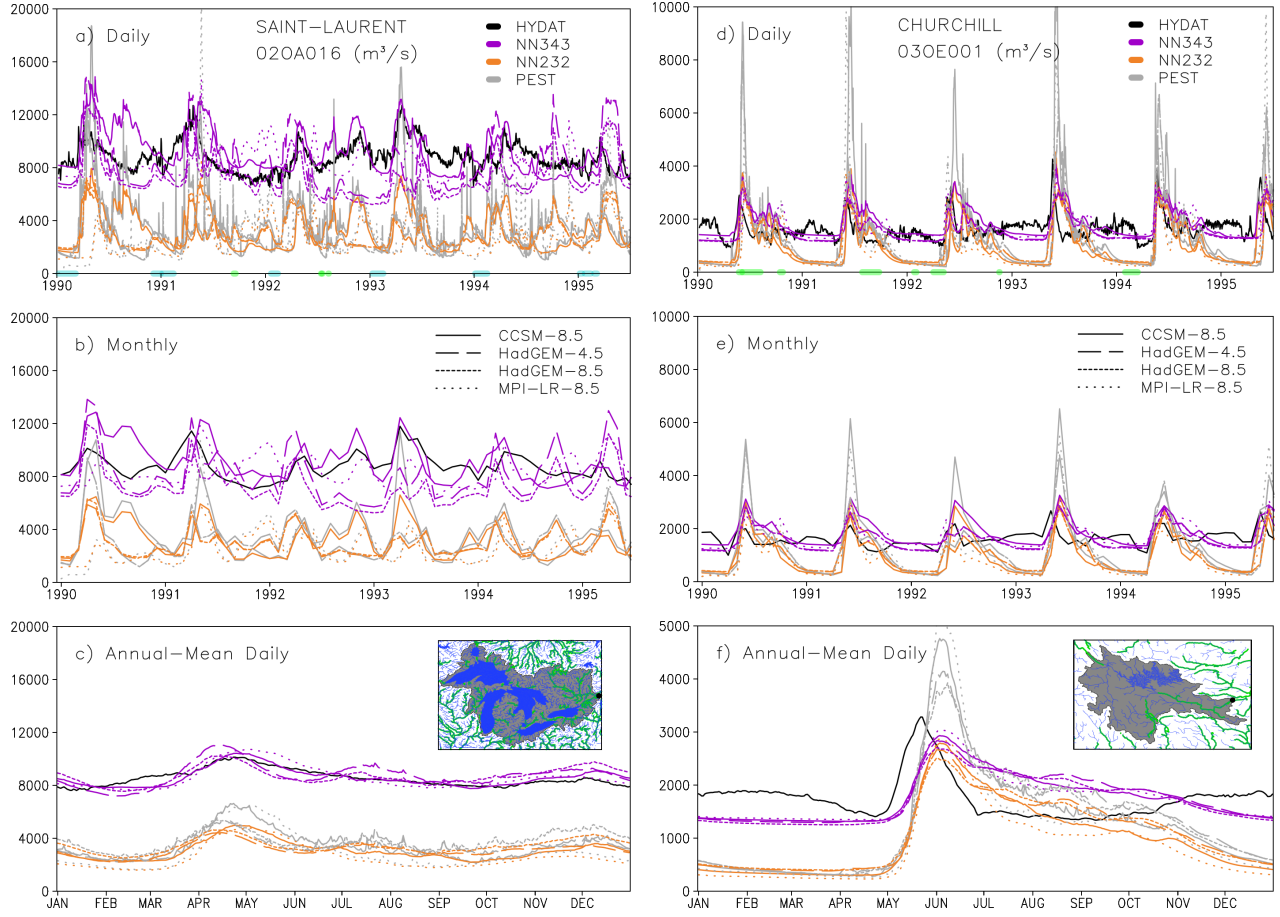


Figure 6: Regulated discharge ($\text{m}^3 \text{s}^{-1}$) of the St. Lawrence River at Lasalle (02OA016, left panels) and the Churchill River above Upper Muskrat Falls (03OE001, right panels) at a,d) daily and b,e) monthly intervals during 1990-1995, and c,f) as annual averages for each day of the year between 1990 and 2022. Shown are the HyDAT (black), PEST (grey), NN232 (orange), and NN343 (purple) representations for the CCSM-4 SSP5-8.5 (solid), HadGEM2 SSP2-4.5 (long dash) and SSP5-8.5 (short dash), and MPI-ESM1.2-LR SSP5-8.5 (dotted) simulations. Insets (c,f) depict station location (black dot) and upstream catchment (grey shading), with WRF-Hydro rivers and lakes (blue) and wide rivers (green; [Altenau et al. 2021](#)). Light blue and green shading (a,d abscissae) denote an ice impact on, or estimate of, HyDAT water level, respectively.

Training and testing of NN343 employed ERA5 forcing (1990-2022), and if gains in similarity to HyDAT were obtained, then NN343 was retrained for each CMIP forcing (i.e., with daily streamflow matched by rank). Ultimately, we applied NN343 at about 10% (51/477) of the ocean outlets in Fig. 1, but with ERA5 forcing, we included 183 HyDAT stations with at least 1000 streamflow observations between 1990 and 2022. Some catchments overlapped (Fig. 7) and this did not include stations whose upstream catchment area on the WRF-Hydro and HydroSHEDS routing grids differed by more than a factor of 1.2. Two NN343 calibrations were trained and tested in parallel, by splitting 604449 observations from even years and 631995 observations from odd

years (i.e., trained using one set and tested using the other).

183 HYDAT Stations and WRF-Hydro Catchments

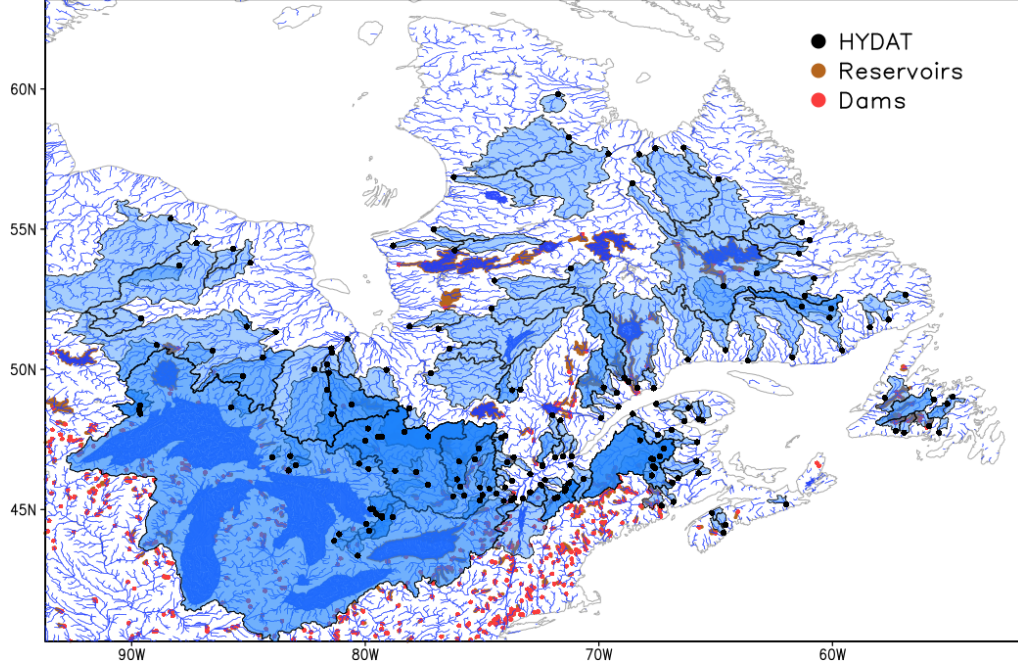


Figure 7: Catchments (overlapping light blue shading) upstream of 183 HyDAT stations (black dots), where 1236444 daily observations are available between 1990 and 2022. Also shown is the 2-km WRF-Hydro river and lake network (dark blue), and reservoirs (brown) and dams (red), as given by [Lehner et al. \(2011\)](#).

Table 5 confirms the NN343 gains in similarity, with odd-year (left columns) and even-year (right columns) test results being nearly equivalent. A convenient summary is given by the number of satisfactory stations ([Moriassi et al. 2015](#)). With PEST and NN232 calibration, we found between 41 and 56 stations (22% to 31%) to be satisfactory, and by including the NN343 calibration, station number more than doubled (46% to 68%; bold values). This prompted a second attempt to find a uniform calibration for all natural flows across eastern Canada (gauged or not), but unfortunately, we found no average gain when training a single NN343 calibration simultaneously at a group

of 85 HyDAT stations (not shown). Thus, NN343 training focused on individual HyDAT stations, and specifically, any whose upstream catchment covered at least 40% of the corresponding ocean outlet catchment (Fig. 8). This yielded 51 HyDAT stations that we could use to calibrate ocean outlets downstream ([Dai and Trenberth 2002](#)).

Satisfac. Stations	DIFF (%)	NSE	COR	Avg.	Satisfac. Stations	DIFF (%)	NSE	COR
14/41/ 84	61/46/ 9	-9/-3/ 0.48	0.58/0.62/ 0.68	Day	10/43/ 90	62/46/ 8	-8/-3/ 0.43	0.58/0.62/ 0.66
37/52/ 113	61/46/ 9	-9/-3/ 0.57	0.69/0.68/ 0.75	Mon.	40/55/ 124	62/46/ 8	-7/-3/ 0.53	0.69/0.69/ 0.74
33/51/ 112	61/46/ 9	-7/-3/ 0.62	0.67/0.69/ 0.76	Ann.	34/56/ 125	62/46/ 8	-10/-4/ 0.57	0.68/0.70/ 0.74

Table 5: Similarity of ERA5-forced streamflow to HyDAT, as in Table 4, but for the 183 stations of Fig. 7 after calculating daily, monthly, and annual-mean (daily) averages. Neural network training and testing employ even- and odd-year streamflow (leftmost columns), and odd- and even-year streamflow (rightmost columns), respectively. Values are shown for PEST/NN232/NN343 and bold denotes the calibration with greatest similarity between WRF-Hydro and HyDAT.

51 Ocean Outlets and Upstream HYDAT Stations

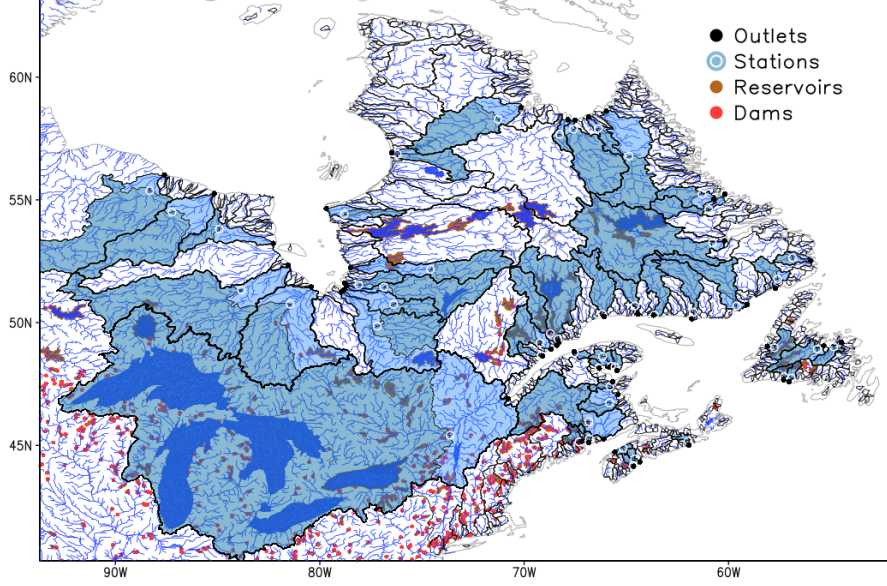


Figure 8: As in Fig. 7, but for 51 ocean outlets (black dots) whose nearest inland HyDAT stations (white circles) have upstream catchment areas (grey overlap) that are at least 40% of the ocean outlet catchment areas (light blue). A total of 366743 daily observations are available between 1990 and 2022.

Satisfac. Stations	DIFF (%)	NSE	COR	Avg.	Satisfac. Stations	DIFF (%)	NSE	COR
4/15/ 26	30/20/ 7	-1/0/ 0.4	0.62/0.68/0.68	Day	4/17/ 27	29/20/ 8	-1/ 0/ 0.4	0.62/0.69/0.69
10/18/ 33	29/20/ 6	-1/0/ 0.5	0.75/0.75/ 0.76	Mon.	14/19/ 35	29/20/ 8	-1/ 0/ 0.5	0.76/0.76/ 0.77
10/18/ 36	28/19/ 7	-1/0/ 0.5	0.72/0.75/0.75	Ann.	12/20/ 35	29/19/ 8	-2/-1/ 0.5	0.75/0.78/0.78

Table 6: As in Table 5, but for the 51 HyDAT stations of Fig. 8. Representations shown are the PEST/NN232/NN343-seasonal values, where the latter is a seasonal CMIP calibration (see text).

We performed one final test of NN343 to examine the impact of streamflow matching by rank (Section 3.d). This employed ERA5 forcing and the 51 HyDAT stations, and during training, the daily streamflow of WRF-Hydro was matched by rank to that of HyDAT, while the order of monthly and annual-mean values were unchanged. In spite of this partial resorting, gains in HyDAT similarity (Table 6) were comparable to gains for all 183 stations (Table 5), with over half of the 51 stations being satisfactory.

All steps in Table 1 were taken to produce the four calibrated projections of eastern Canadian discharge. For each of the CCSM-4, HadGEM2, and MPI-ESM1.2-LR models, a three-year WRF-Hydro spinup was followed by simulations from 1990 to 2100 using PEST parameters, with the NN232 calibration at all 477 ocean outlets, and a NN343 calibration at 51 outlets. The discharge from all rivers between the Severn and St. Croix was then summed, and Figure 9 shows the annual and decadal averages, with peak dis-

charge in May of about $10^5 \text{ m}^3 \text{ s}^{-1}$. As expected, each simulation captured increasing annual discharge (Fig. 9a-d), and as others have found (e.g., [Bonsal et al. 2019](#); [Stadnyk et al. 2021](#)), the decadal averages revealed increasing low flow during the cold season and an earlier peak discharge in spring (Fig. 9e-p). The calibration of each CMIP simulation to a common set of observational references was expected to yield greater precision, and this was also confirmed. Without calibration, the daily discharge mean and standard deviation are more disparate across the four models (Fig. 9m-p), whereas with calibration, the CMIP simulations share a mean of $56 \times 10^3 \text{ m}^3 \text{ s}^{-1}$ and a more similar variance (Fig. 9e-h). There are also striking differences among the four discharge simulations, even after calibration. However, attribution of the reduced seasonality of the HadGEM2 simulations in a hydroclimatic assessment that includes CCSM-4 and MPI-ESM1.2-LR is beyond our present scope.

5 Discussion

This climate configuration of WRF-Hydro employs lower spatiotemporal resolution, but after calibration to historical records (Pellerin and Nzokou Tanekou 2020; de Rham et al. 2020; Water Survey of Canada 2023), our streamflow predictions compare favourably to similar high latitude modelling efforts. For instance, the spatially uniform calibration given by PEST and NN232 yields monthly gains in similarity on par with those of Stadnyk et al. (2021), who found 30% of stations to be satisfactory. Moreover, at catchments where an individual NN343 calibration could also be performed, satisfactory stations more than doubled to 62%-68% (Tables 5 and 6).

We treat NN232 and NN343 as extensions of physical models that address processes like streamflow buffering and regulation, but unlike the nine WRF-Hydro parameters of Table 2, we do not associate any of the 23 or 39 parameters with specific processes because our densely connected structures are ad hoc. When physical processes are not apparent, neural networks are adaptive and convenient, but their use seems justifiable because they do well at *parameterizing* non-linear associations (Section 3.d). For instance, the 1990-2100 WRF-Hydro trends in Fig. 9a-d appear to be shifted after each calibration step by a constant value. On one hand, this means that calibrated trends are well behaved (Maraun 2016) and an analysis of the uncalibrated trends would be equivalent (cf. Stadnyk et al. 2021). On the other hand, Stadnyk et al. (2021) point out that regulation is expected to have an impact on trends. Thus, we would caution that a) relatively simple neural networks like NN232 and NN343 seem to provide well behaved process parameterizations for 1990-2022, and b) we are making the conventional assumption that such parameterizations can be applied well beyond 2022 (Maraun 2016).

We emphasize hydrologic model output (ocean forcing) in this study, but equal emphasis on the input (atmospheric forcing) is needed in an Earth system modelling context. In lieu of our simple adjustment of atmospheric forcing (Section 3.b), either a neural network calibration (Section 3.d) or bias correction (Cannon 2018) can be considered. Moreover, in lieu of neural network calibration of ocean forcing (streamflow), bias correction can also be considered. Seeking to preserve intervariable dependence is advantageous (Cannon 2018), but bias correction also reorders slightly the sequence of synoptic events, which can shorten their duration (Cannon 2016). No attempt was made to preserve intervariable dependence here. Although NN343 also reorders daily streamflow (i.e., by matching rank), this is only done during training, so unlike bias correction, its input and output time sequence is the same. Following Cannon (2018),

both methods preserve trends of increasing annual discharge (Fig. 9a-d) and seem well behaved (Maraun 2016).

A balanced emphasis on the internal calibration of WRF-Hydro also has merit, yet we opted not to allow PEST to adjust more than nine WRF-Hydro parameters, including Manning’s roughness coefficients for rivers (cf. Wang et al. 2019), or to allow the WRF-Hydro parameters to vary spatially (Mendoza et al. 2015; Rafieei Nasab et al. 2020; Gochis et al. 2021). However, each calibration depends on those before it, and we expect that NN232 and NN343 compensate in part for the tuning that could be done internally to WRF-Hydro, say, to represent regulation and buffering by small lakes (Déry et al. 2018; Stadnyk et al. 2020). In this study, we also address a less obvious compensation between data and process models, where it is common to develop parameterizations for WRF-Hydro (or like NN343), and less common to develop the data models that we use to select their parameterization values, like by (1) and (2). In spite of the seemingly different calibration steps that we employ, there may be some benefit to expressing data models in a way that allows their fundamental similarities (Table 1) and differences (Beven 2021) to be recognized within a common and familiar framework (Appendix).

6 Conclusions

A calibration of WRF-Hydro with respect to eastern Canadian streamflow observations from 1990-2022 is performed in support of regional hydroclimate simulations through 2100. The WRF-Hydro model (Gochis et al. 2021) is applicable over a wide range of spatiotemporal scales and benefits from an efficient automatic calibration (Doherty 2015; Wang et al. 2019) of its model parameters (Rafieei Nasab et al. 2020). Starting with a relatively low resolution (50-km/2-km) grid and (6-h ERA5) atmospheric forcing, we modify watershed boundaries of the Eilander et al. (2021) digital elevation model to more easily relate predicted and observed streamflow at gauging stations. Following Doherty (2015), we then use PEST to identify nine spatially invariant WRF-Hydro parameters. Because some parameter estimates are close to a limit in their range, however, we cannot identify a uniform model representation of natural flow through the eastern Canadian river network.

By way of committing to a calibration by individual (regulated) watershed and CMIP forcing (Taylor et al. 2012; Eyring et al. 2016), we calibrate WRF-Hydro streamflow using a pair of neural networks (NN232 and NN343) that build on the PEST calibration. First, gains in similarity to HyDAT stream-

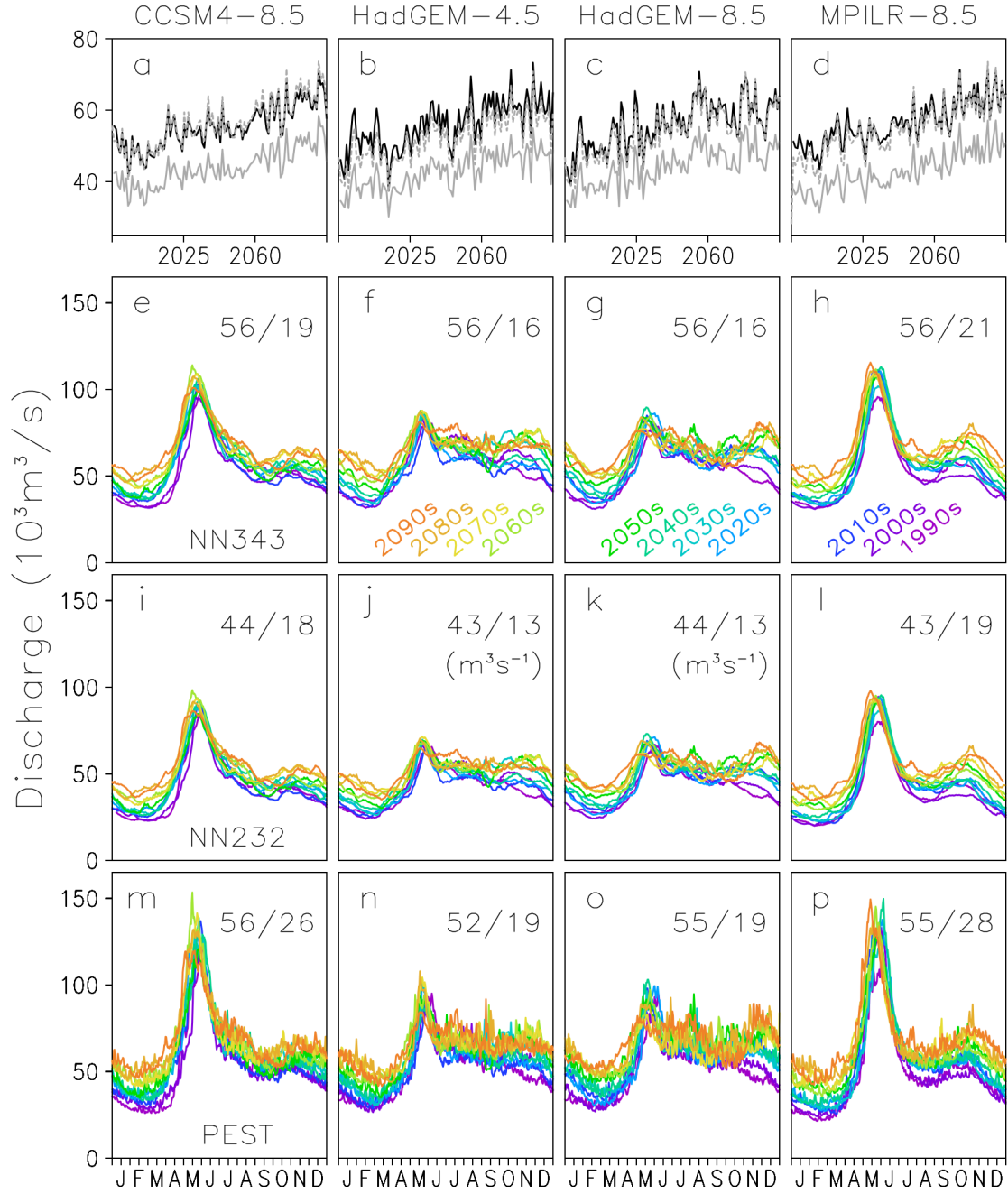


Figure 9: Simulated 1990-2100 discharge ($10^3 \text{ m}^3 \text{ s}^{-1}$) for the 477 eastern Canadian rivers between the Severn and St. Croix (Fig. 1) using downscaled CMIP forcing from CCSM-4 SSP5-8.5 (left column), HadGEM2 SSP2-4.5 and SSP5-8.5 (center-left and right), and MPI-ESM1.2-LR SSP5-8.5 (right column). Shown are a-d) annual averages and e-p) daily averages for decades (colours) for NN343 (e-h; a-d grey dashed lines), NN232 (i-l; a-d grey lines), and PEST (m-p; a-d black lines) calibrations. Panels (e-p) include mean/standard deviation of daily discharge at upper right.

flow observations (Pellerin and Nzokou Tanekou 2020; de Rham et al. 2020; Water Survey of Canada 2023) are confirmed for NN232, which is trained to reduce strong peaks in seasonal and daily discharge simulations. With over 10^6 streamflow observations during 1990-2022, gains in similarity are then confirmed using PEST, NN232, and NN343 calibration, where NN343 is trained at 183 HyDAT stations. An experiment to train NN343 jointly at 85 stations does not yield an average gain in similarity.

Training of NN343 is performed separately for four CMIP-forcing simulations and at 51 HyDAT stations that permit a downstream adjustment of discharge, following Dai and Trenberth (2002). This training is novel in that CMIP simulations are calibrated directly to HyDAT observations, as NN343 employs three input and output nodes. Similar to Freilich and Challenor (1994), training employs a sorting of WRF-Hydro and HyDAT streamflow that are matched by rank, but only for the daily input/output node. A seasonal calibration is thus obtained by not sorting at the other two nodes (i.e., the monthly and annual averages). This yields gains in similarity at the HyDAT stations that are equivalent to those of 183 stations, with over half the 51 stations being satisfactory (Moriasi et al. 2015; Stadnyk et al. 2021).

The resulting hydrologic data-calibration steps are applied to obtain eastern Canadian freshwater discharge through the 477 WRF-Hydro ocean outlets for each of the four CMIP models. Whereas WRF-Hydro with PEST parameters yields strong seasonal and daily peaks relative to HyDAT, and these peaks are smoothed by NN232, the separate NN343 calibration at 51 ocean outlets yields relatively precise annual variations and interannual trends for all CMIP forcings. This provides further support for an increasing low flows during future cold seasons and an earlier peak discharge in future spring seasons (Bonsal et al. 2019; Stadnyk et al. 2021).

Acknowledgements

We thank Adam Drozdowski, Zhenxia Long, Bash Toulany, and two anonymous reviewers who provided thoughtful comments and a significantly updated presentation structure. Funding was provided by the Competitive Science Research Fund (CSRF) of Fisheries and Oceans Canada (DFO). All models and data have been freely provided, and we thank the WRF-Hydro (NCAR), MERIT (University of Tokyo, Vrije Universiteit Amsterdam), HydroSHEDS (WWF, McGill University), CMIP (World Climate Research Programme), HyDAT and RHBN (ECCC) model and data development teams. DFO and the Digital Research Alliance of Canada provided computational re-

sources and support. Data processing and visualization employed Julia (Julia Computing Inc., MIT), WhiteBoxTools (University of Guelph), and GrADs (COLA, George Mason University), respectively. Gitlab hosts code shared by the DFO modelling community (MODCOM), including our configuration steps (https://gitlab.com/dfo_modcom/diag.hydrology).

Appendix – A data modelling primer

There are active discussions in the Earth sciences about what we might describe as data modelling within the familiar context of process modelling. Here, we use data models to provide a mathematical framework for calibration and confirmation, including the definition of an “equivalence assumption” and supporting terms. To acknowledge that data modelling and process modelling may be *complementary*, we specify data while not being specific about the hydrologic processes that they refer to. The common notions of association that we sometimes express in words can often be expressed as a data model. In turn, we claim that data models provide a basis for calibration and confirmation, even if it might not be easy to recognize such a foundation within a familiar knowledge system (Beven 2021; Nearing et al. 2016; Kalman 1994). For example, the expression “this watershed boundary is our reference” can be written as a common model, as can all associations that are made in this study.

At each step toward what is observed and expected, we make a particular representation (i.e., predictions or observations) more similar to a selected reference (i.e., an ideal representation) using a data model of the form

$$C = t + \epsilon_c \quad \text{and} \quad U = t + \epsilon_u. \quad (3)$$

Here, C and U are the calibrated and uncalibrated representations (e.g., observed and predicted streamflow) with errors ϵ_c and ϵ_u , respectively. We refer to (3) as a target model if the calibration reference (C) includes error, and otherwise, as a truth model if $\epsilon_c = 0$, and a truth-truth model if $\epsilon_u = 0$ as well.

Glossary of model terms

Bias correction: This is an association of two representations, expressed in terms of the mean, variance, or quantiles of C and U (Ehret et al. 2012; Maraun 2016). Systematic differences in the representations of one Earth system model component and another (or that of a regional model or local observations) generally involve multivariate associations be-

tween C and U (Cannon 2018), and by the truth-truth model, their covariance and quantiles are taken as error free (Cannon 2016).

Data model: We acknowledge the need to explore different types of associations within a mathematical knowledge system by, for example, including the notion of epistemic observational uncertainty (Beven 2021). Clearly, a general framework is desirable (Kalman 1994; Nearing et al. 2016) and it seems worthwhile to consider common expressions like (3) as contributing to such a framework (i.e., where data includes predictions and observations). *Even when no calculations are performed* (Section 3.a,b), a data model provides a mathematical foundation for calibration, as the relationship between predictions and observations assumes such a model, and this can guide a formulation of measurement performance, which in turn, can guide our predictive model adjustments.

Equivalence assumption: Data models may be common, on one hand, but it is important to note that while C and U are related via t , they are expressed separately in (3) because each representation of nature is expected to capture processes somewhat differently (Lorenz 1985; Smith 2006; Parker 2017; Beven 2021). On the other hand, the use of (3) in parameter estimation (Doherty 2015), data assimilation (Mahfouf 1991), machine learning (Kratzert et al. 2019), and model confirmation (Moriassi et al. 2015) typically follows from equating C and U in order to minimize the model-observation difference. We employ this as-

sumption throughout our study.

Knowledge systems: We acknowledge the association of other knowledge systems with the scientific, mathematical, and linguistic systems that we relied on to explore hydrologic aspects in this study. We also acknowledge that these aspects of nature are expressed in knowledge systems other than the ones we are familiar with.

Reference: Any dataset (predictions or observations) might be considered a useful depiction of some aspect of nature. It is convenient in this study to take one representation (the reference) as a temporary proxy of nature, but caution is warranted, as an association of two datasets might only be linear where there is an overlap in their representations (e.g., processes resolved by both). In taking one as a reference, only nonlinear association might be possible where representations do not overlap (e.g., via interactions with unresolved processes; Section 3.d).

Representation: Any dataset (predictions or observations) might be considered an improving depiction of some aspect of nature. A representation is such a depiction (e.g., water level at a gauging station or multivariate data on the WRF-Hydro grid). Even if a familiar representation is the result of many years of development with associations to many datasets, strictly from a metrological point of view, this remains a specific representation with specific associations (Bulgin et al. 2022).

References

- Altenau, E. H., T. M. Pavelsky, M. T. Durand, X. Yang, R. P. d. M. Frasson, and L. Bendezu, 2021: The Surface Water and Ocean Topography (SWOT) Mission River Database (SWORD): A global river network for satellite data products. *Water Resour. Res.*, **57**, 1–15, doi:10.1029/2021WR030054.
- Berg, P., C. Donnelly, and D. Gustafsson, 2018: Near-real-time adjusted reanalysis forcing data for hydrology. *Hydrol. Earth System Sci.*, **22**, 989–1000, doi:10.5194/hess-22-989-2018.
- Beven, K., 2019: Towards a methodology for testing models as hypotheses in the inexact sciences. *Proc. Roy. Soc. A*, **475**, 1–19, doi:10.1098/rspa.2018.0862.
- Beven, K., 2021: An epistemically uncertain walk through the rather fuzzy subject of observation and model uncertainties. *Hydrol. Processes*, **35**, 1–9, doi:10.1002/hyp.14012.
- Bonsal, B. R., D. L. Peters, F. Seglenieks, A. Rivera, and A. Berg, 2019: Changes in freshwater availability across Canada, Chapter 6 of *Canada’s Changing Climate Report*, E. Bush and D. S. Lemmen, Eds., Government of Canada, Ottawa, Ontario, p. 261–342, (accessed April 2024 at <https://changingclimate.ca/CCCR2019>).
- Bulgin, C. E., C. M. Thomas, J. A. Waller, and E. R. Woolliams, 2022: Representation uncertainty in the Earth sciences. *Earth Space Sci.*, **9**, 1–7, doi:10.1029/2021EA002129.
- Bush, E., and D. S. Lemmen, 2019: Canada’s Changing Climate Report, Government of Canada, Ottawa, Ontario, 444 pp., (accessed April 2024 at <https://changingclimate.ca/CCCR2019>).

- Cannon, A. J., 2016: Multivariate bias correction of climate model output: Matching marginal distributions and intervariable dependence structure. *J. Climate*, **29**, 7045–7064, doi:10.1175/JCLI-D-15-0679.1.
- Cannon, A. J., 2018: Multivariate quantile mapping bias correction: An N-dimensional probability density function transform for climate model simulations of multiple variables. *Climate Dyn.*, **50**, 31–49, doi:10.1007/s00382-017-3580-6.
- Clevert, D.-A., T. Unterthiner, and S. Hochreiter, 2015: Fast and accurate deep network learning by exponential linear units (ELUs), arXiv:1511.07289 [cs.LG].
- Collins, W. J., N. Bellouin, M. Doutriaux-Boucher, N. Gedney, P. Halloran, T. Hinton, J. Hughes, C. D. Jones, M. Joshi, S. Liddicoat, G. Martin, F. O’Connor, J. Rae, C. Senior, S. Sitch, I. Totterdell, A. Wiltshire, and S. Woodward, 2011: Development and evaluation of an Earth-System model – HadGEM2. *Geosci. Model Dev.*, **4**, 1051–1075, doi:10.5194/gmd-4-1051-2011.
- Dai, A., and K. E. Trenberth, 2002: Estimates of freshwater discharge from continents: Latitudinal and seasonal variations. *J. Hydrometeor.*, **3**, 660–687, doi:10.1175/1525-7541(2002)003<0660:EOFDFC>2.0.CO;2.
- Dai, A., T. Qian, K. E. Trenberth, and J. D. Milliman, 2009: Changes in continental freshwater discharge from 1948 to 2004. *J. Climate*, **22**, 2773–2792, doi:10.1175/2008JCLI2592.1.
- de Rham, L., Y. Dibike, S. Beltaos, D. Peters, B. Bonsal, and T. Prowse, 2020: A Canadian river ice database from the National Hydrometric Program archives. *Earth Syst. Sci. Data*, **12**, 1835–1860, doi:10.5194/essd-12-1835-2020.
- Dee, D. P., 2005: Bias and data assimilation. *Quart. J. Roy. Meteor. Soc.*, **131**, 3323–3343, doi:10.1256/qj.05.137.
- Derksen, C., D. Burgess, C. Duguay, S. Howell, L. Mudryk, S. Smith, C. Thackeray, and M. Kirchmeier-Young, 2019: Changes in snow, ice, and permafrost across Canada, Chapter 5 of *Canada’s Changing Climate Report*, E. Bush and D. S. Lemmen, Eds., Government of Canada, Ottawa, Ontario, p. 194–260.
- Déry, S. J., T. A. Stadnyk, M. K. MacDonald, K. A. Koenig, and C. Guay, 2018: Flow alteration impacts on Hudson Bay river discharge. *Hydrol. Processes*, **32**, 3576–3587, doi:10.1002/hyp.13285.
- Doherty, J., 2015: *Calibration and Uncertainty Analysis for Complex Environmental Models*, with PEST: Model Independent Parameter Estimation, User Manual, 7th ed., available at <https://pesthomepage.org> (accessed May 2023), Watermark Numerical Computing, Brisbane, Australia, 227 pp.
- Ehret, U., E. Zehe, V. Wulfmeyer, K. Warrach-Sagi, and J. Liebert, 2012: Should we apply bias correction to global and regional climate model data? *Hydrol. Earth System Sci.*, **16**, 3391–3404, doi:10.5194/hess-16-3391-2012.
- Eilander, D., W. van Verseveld, D. Yamazaki, A. Weerts, H. C. Winsemius, and P. J. Ward, 2021: A hydrography upscaling method for scale-invariant parametrization of distributed hydrological models. *Hydrol. Earth System Sci.*, **25**, 5287–5313, doi:10.5194/hess-25-5287-2021.
- Eyring, V., S. Bony, G. A. Meehl, C. A. Senior, B. Stevens, R. J. Stouffer, and K. E. Taylor, 2016: Overview of the Coupled Model Intercomparison Project Phase 6 (CMIP6) experimental design and organization. *Geosci. Model Dev.*, **9**, 1937–1958, doi:10.5194/gmd-9-1937-2016.
- Flato, G., N. Gillett, V. Arora, A. Cannon, and J. Anstey, 2019: Modelling future climate change, Chapter 3 of *Canada’s Changing Climate Report*, E. Bush and D. S. Lemmen, Eds., Government of Canada, Ottawa, Ontario, p. 74–111, (accessed April 2024 at <https://changingclimate.ca/CCCR2019>).
- Freilich, M. H., and P. G. Challenor, 1994: A new approach for determining fully empirical altimeter wind speed model functions. *J. Geophys. Res.*, **99**, 25051–25062, doi:10.1029/94JC01996.
- Gochis, D. J., M. Barlage, R. Cabell, M. Casali, A. Dugger, K. FitzGerald, M. McAllister, J. McCreight, A. Rafieei Nasab, L. Read, K. Sampson, D. Yates, and Y. Zhang, 2021: The NCAR WRF-Hydro modeling system technical description, (Version 5.2.0), NCAR Technical Note, 108 pp., available at <https://ral.ucar.edu/sites/default/files/public/projects/wrf-hydro/technical-description-user-guide/wrf-hydrov5.2technicaldescription.pdf> (accessed October 9, 2023).

- Greenan, B. J. W., T. S. James, J. W. Loder, P. Pepin, K. Azetsu-Scott, D. Ianson, R. C. Hamme, D. Gilbert, J.-É. Tremblay, X. L. Wang, and W. Perrie, 2019: Changes in oceans surrounding Canada, Chapter 7 of *Canada’s Changing Climate Report*, E. Bush and D. S. Lemmen, Eds., Government of Canada, Ottawa, Ontario, p. 343–423, (accessed April 2024 at <https://changingclimate.ca/CCCR2019>).
- Hersbach, H., B. Bell, P. Berrisford, S. Hirahara, A. Horányi, J. Muñoz-Sabater, J. Nicolas, C. Peubey, R. Radu, D. Schepers, A. Simmons, C. Soci, S. Abdalla, X. Abellan, G. Balsamo, P. Bechtold, G. Biavati, J. Bidlot, M. Bonavita, G. De Chiara, P. Dahlgren, D. Dee, M. Diamantakis, R. Dragani, J. Flemming, R. Forbes, M. Fuentes, A. Geer, L. Haimberger, S. Healy, R. J. Hogan, E. Hólm, M. Janisková, S. Keeley, P. Laloyaux, P. Lopez, C. Lupu, G. Radnoti, P. de Rosnay, I. Rozum, F. Vamborg, S. Villaume, and J.-N. Thépaut, 2020: The ERA5 global reanalysis. *Quart. J. Roy. Meteor. Soc.*, **146**, 1999–2049, doi:10.1002/qj.3803.
- Innes, M., E. Saba, K. Fischer, D. Gandhi, M. C. Rudilosso, N. M. Joy, T. Karmali, A. Pal, and V. B. Shah, 2018: Fashionable modelling with Flux, arXiv:1811.01457 [cs.PL].
- IPCC, 2013: Summary for Policymakers. In: *Climate Change 2013: The Physical Science Basis. Contribution of Working Group I to the Fifth Assessment Report of the Intergovernmental Panel on Climate Change*, T.F. Stocker, D. Qin, G.-K. Plattner, M. Tignor, S.K. Allen, J. Boschung, A. Nauels, Y. Xia, V. Bex and P.M. Midgley, Eds., Cambridge University Press.
- Jacquelin, J., 2014: Régressions et équations intégrales (accessed July 2024 at https://scikit-guess.readthedocs.io/en/latest/_downloads/4cd313a50f7e08ab81758ce0bd661bc3/Regressions-et-equations-integrales.pdf).
- Kalman, R. E., 1994: Randomness reexamined. *Modeling, Identification and Control*, **15**, 141–151, doi:10.4173/mic.1994.3.3.
- Kratzert, F., D. Klotz, G. Shalev, G. Klambauer, S. Hochreiter, and G. Nearing, 2019: Towards learning universal, regional, and local hydrological behaviors via machine learning applied to large-sample datasets. *Hydrol. Earth System Sci.*, **23**, 5089–5110, doi:10.5194/hess-23-5089-2019.
- Lehner, B., K. Verdin, and A. Jarvis, 2008: New global hydrography derived from spaceborne elevation data. *Eos Trans. AGU*, **89**, 93–94, doi:10.1029/2008EO100001.
- Lehner, B., C. R. Liermann, C. Revenga, C. Vörösmarty, B. Fekete, P. Crouzet, P. Döll, M. Endejan, K. Frenken, J. Magome, C. Nilsson, J. Robertson, R. Rödel, N. Sindorf, and D. Wisser, 2011: High-resolution mapping of the world’s reservoirs and dams for sustainable river-flow management. *Front. Ecol. Environ.*, **9**, 494–502, doi:10.1890/100125.
- Lorenz, E. N., 1985: The growth of errors in prediction, *Proceedings of the International School of Physics Enrico Fermi*, M. Ghil, R. Benzi, and G. Parisi, Eds., Course 88 on Turbulence and Predictability in Geophysical Fluid Dynamics and Climate Dynamics, North Holland: Amsterdam, 243–265.
- Mahfouf, J.-F., 1991: Analysis of soil moisture from near-surface parameters: A feasibility study. *J. Appl. Meteor.*, **30**, 1534–1547, doi:10.1175/1520-0450(1991)030<1534:AOSMFN>2.0.CO;2.
- Maraun, D., 2016: Bias correcting climate change simulations - a critical review. *Curr. Clim. Change Rep.*, **2**, 211–220, doi:10.1007/s40641-016-0050-x.
- Mauritsen, T., J. Bader, T. Becker, J. Behrens, M. Bittner, R. Brokopf, V. Brovkin, M. Claussen, T. Crueger, M. Esch, I. Fast, S. Fiedler, D. Fläschner, V. Gayler, M. Giorgetta, D. S. Goll, H. Haak, S. Hagemann, C. Hedemann, C. Hohenegger, T. Ilyina, T. Jahns, D. Jimenéz-de-la-Cuesta, J. Jungclaus, T. Kleinen, S. Kloster, D. Kracher, S. Kinne, D. Kleberg, G. Lasslop, L. Kornblueh, J. Marotzke, D. Matei, K. Meraner, U. Mikolajewicz, K. Modali, B. Möbis, W. A. Müller, J. E. M. S. Nabel, C. C. W. Nam, D. Notz, S.-S. Nyawira, H. Paulsen, K. Peters, R. Pincus, H. Pohlmann, J. Pongratz, M. Popp, T. J. Raddatz, S. Rast, R. Redler, C. H. Reick, T. Rohrschneider, V. Schemann, H. Schmidt, R. Schnur, U. Schulzweida, K. D. Six, L. Stein, I. Stemmler, B. Stevens, J.-S. von Storch, F. Tian, A. Voigt, P. Vrese, K.-H. Wieners, S. Wilenskijeld, and E. R. Alexander Winkler and, 2019: Developments in the MPI-M Earth System Model version 1.2 (MPI-ESM1.2) and its response to increasing CO₂. *J. Adv. Model. Earth Sys.*, **11**, 998–1038, doi:10.1029/2018MS001400.

- Meehl, G. A., W. M. Washington, J. M. Arblaster, A. Hu, H. Teng, C. Tebaldi, B. N. Sanderson, J.-F. Lamarque, A. Conley, W. G. Strand, and J. B. White III, 2012: Climate system response to external forcings and climate change projections in CCSM4. *J. Climate*, **25**, 3661–3683, doi:10.1175/JCLI-D-11-00240.1.
- Mendoza, P. A., M. P. Clark, M. Barlage, B. Rajagopalan, L. Samaniego, G. Abramowitz, and H. Gupta, 2015: Are we unnecessarily constraining the agility of complex process-based models? *Water Resour. Res.*, **51**, 716–728, doi:10.1002/2014WR015820.
- Messenger, M. L., B. Lehner, G. Grill, I. Nedeva, and O. Schmitt, 2016: Estimating the volume and age of water stored in global lakes using a geo-statistical approach. *Nat. Commun.*, **7**, 1–11, doi:10.1038/ncomms13603.
- Moriasi, D. N., M. W. Gitau, N. Pai, and P. Daggupati, 2015: Hydrologic and water quality models: Performance measures and evaluation criteria. *Trans. ASABE*, **58**, 1763–1785, doi:10.13031/trans.58.10715.
- Morin, J., and O. Champoux, 2006: Integrated modelling of the physical processes and habitats of the St. Lawrence River, Chapter 3 of *Water Availability Issues for the St. Lawrence River: An Environmental Synthesis*, A. Talbot, Ed., Environment Canada, 22–37.
- Nearing, G. S., Y. Tian, H. V. Gupta, M. P. Clark, K. W. Harrison, and S. V. Weijs, 2016: A philosophical basis for hydrological uncertainty. *Hydrol. Sci. J.*, **61**, 1666–1678, doi:10.1080/02626667.2016.1183009.
- O’Neill, B. C., E. Kriegler, K. L. Ebi, E. Kemp-Benedict, K. Riahi, D. S. Rothman, B. J. van Ruijven, D. P. van Vuuren, J. Birkmann, K. Kok, M. Levy, and W. Solecki, 2017: The roads ahead: Narratives for shared socioeconomic pathways describing world futures in the 21st century. *Global Environ. Change*, **42**, 169–180, doi:10.1016/j.gloenvcha.2015.01.004.
- Parker, W. S., 2017: Computer simulation, measurement, and data assimilation. *Brit. J. Phil. Sci.*, **68**, 273–304, doi:10.1093/bjps/axv037.
- Pellerin, J., and F. Nzokou Tanekou, 2020: Reference Hydrometric Basin Network update, Environment and Climate Change Canada, Gatineau, Québec, 30 pp., available at https://collaboration.cmc.ec.gc.ca/cmc/hydrometrics/www/RHBN/RHBN_EN.pdf (accessed October 10, 2023).
- Rafieei Nasab, A., L. Karsten, A. Dugger, K. FitzGerald, R. Cabell, D. Gochis, D. Yates, K. Sampson, J. McCreight, L. Read, Y. Zhang, and M. McAllister, 2020: Overview of National Water Model calibration: General strategy and optimization, NCAR WRF-Hydro community training material (November 6), 28 slides, available at <https://ral.ucar.edu/sites/default/files/public/projects/wrf-hydro/training-materials/calibrationnov2020-arezoo.pdf> (accessed October 2, 2023).
- Rumelhart, D. E., G. E. Hinton, and R. J. Williams, 1986: Learning representations by back-propagating errors. *Nature*, **323**, 533–536, doi:10.1038/323533a0.
- Schmidt, G. A., D. Bader, L. J. Donner, G. S. Elsaesser, J.-C. Golaz, C. Hannay, A. Molod, R. B. Neale, and S. Saha, 2017: Practice and philosophy of climate model tuning across six US modeling centers. *Geosci. Model Dev.*, **10**, 3207–3223, doi:10.5194/gmd-10-3207-2017.
- Smith, L. A., 2006: Predictability past, predictability present, *Predictability of Weather and Climate*, T. Palmer and R. Hagedorn, Eds., Cambridge University Press, 217–250, doi:10.2307/j.ctv1pnc1q9.10.
- Stadnyk, T. A., M. K. MacDonald, A. Tefs, S. J. Déry, K. Koenig, D. Gustafsson, K. Isberg, and B. Arheimer, 2020: Hydrological modeling of freshwater discharge into Hudson Bay using HYPE. *Elem. Sci. Anth.*, **8**, 1–18, doi:10.1525/elementa.439.
- Stadnyk, T. A., A. Tefs, M. Broesky, S. J. Déry, P. G. Myers, N. A. Ridenour, K. Koenig, L. Vonderbank, and D. Gustafsson, 2021: Changing freshwater contributions to the Arctic: A 90-year trend analysis (1981–2070). *Elem. Sci. Anth.*, **9**, 1–26, doi:10.1525/elementa.2020.00098.
- Stiles, B. W., R. E. Danielson, W. L. Poulsen, M. J. Brennan, S. M. Hristova-Veleva, T.-P. Shen, and A. G. Fore, 2014: Optimized tropical cyclone winds from QuikSCAT: A neural network approach. *IEEE Trans. Geosci. Remote Sens.*, **52**, 7418–7434, doi:10.1109/TGRS.2014.2312333.

- Taylor, K. E., R. J. Stouffer, and G. A. Meehl, 2012: An overview of CMIP5 and the experiment design. *Bull. Amer. Meteor. Soc.*, **93**, 485–498, doi:10.1175/JTECH-D-12-00008.1.
- Wang, J., C. Wang, V. Rao, A. Orr, E. Yan, and R. Kotamarthi, 2019: A parallel workflow implementation for PEST version 13.6 in high-performance computing for WRF-Hydro version 5.0: A case study over the midwestern United States. *Geosci. Model Dev.*, **12**, 3523–3539, doi:10.5194/gmd-12-3523-2019.
- Water Survey of Canada, 2023: The National Water Data Archive (HyDAT, updated on October 24, 2022), Environment and Climate Change Canada, available at <https://collaboration.cmc.ec.gc.ca/cmc/hydrometrics/www> (accessed November 9, 2022).
- Yamazaki, D., D. Ikeshima, J. Sosa, P. D. Bates, G. H. Allen, and T. M. Pavelsky, 2019: MERIT Hydro: A high-resolution global hydrography map based on latest topography dataset. *Water Resour. Res.*, **55**, 5053–5073, doi:10.1029/2019WR024873.
- Zhang, M., W. Perrie, and Z. Long, 2019a: Sensitivity study of North Atlantic summer cyclone activity in dynamical downscaled simulations. *J. Geophys. Res. Atmos.*, **124**, 7599–7616, doi:10.1029/2018JD029766.
- Zhang, X., G. Flato, M. Kirchmeier-Young, L. Vincent, H. Wan, X. Wang, R. Rong, J. Fyfe, G. Li, and V. V. Kharin, 2019b: Changes in temperature and precipitation across Canada, Chapter 4 of *Canada’s Changing Climate Report*, E. Bush and D. S. Lemmen, Eds., Government of Canada, Ottawa, Ontario, p. 112–193, (accessed April 2024 at <https://changingclimate.ca/CCCR2019>).